Superlong β-$AgVO_3$ Nanoribbons: High-Yield Synthesis by a Pyridine-Assisted Solution Approach, Their Stability, Electrical and Electrochemical Properties

Ji-Ming Song, Yun-Zhi Lin, Hong-Bin Yao, Feng-Jia Fan, Xiao-Guang Li, and Shu-Hong Yu*

Division of Nanomaterials and Chemistry, Hefei National Laboratory for Physical Sciences at Microscale, Departments of Chemistry and Physics, University of Science and Technology of China, Hefei, Anhui 230026, People's Republic of China

ABSTRACT Monoclinic β-silver vanadate (β-$AgVO_3$) nanoribbons with widths of 300—600 nm, thicknesses of *ca.* 40 nm, and lengths of 200—300 μm can be easily synthesized in high yield directly from a hydrothermal reaction between V_2O_5 and $AgNO_3$ in a solution containing a small amount of pyridine. The results demonstrated that the formation of single-crystal $AgVO_3$ nanoribbons is strongly dependent on the reaction temperature, especially, the presence of pyridine and its dosage. A possible growth mechanism of single-crystal $AgVO_3$ nanoribbons has been proposed. Exposure of the nanoribbons to electron beam will easily result in the formation of Ag nanoparticles embedded *in situ* on the backbone of the nanoribbons, making the nanoribbons potentially useful as efficient catalyst support. The electrical conductivity of an individual single-crystal β-$AgVO_3$ nanoribbon exhibits nonlinear and symmetric current/voltage (*I*—*V*) characteristics for bias voltages in the range of −6 to 6 V.

KEYWORDS: β-silver vanadate · nanoribbons · hydrothermal synthesis · stability · conductivity · electrochemical performance

Since the discovery of semiconducting oxide nanoribbons, a variety of inorganic materials of nanoribbons/ribbons have been synthesized and characterized because of their distinctive geometries, novel physical and chemical properties, and potential applications in electronics, optoelectronics, sensors, and the biological sciences.[1−5] Recently, vanadium oxides and vanadium oxide related compounds have received special attention because of their unique physical and chemical properties, such as electrochromic devices, cathodic electrodes for lithium batteries, catalysts, gas sensors, and so on.[6−9] Silver vanadium oxide (SVO) is the cathode active material in lithium primary batteries for implantable cardioverter defibrillators owing to its high gravimetric/volumetric energy densities.[10] Over the past years, there have been some reports on the synthesis of SVO nanomaterials. $AgVO_3$ is a typical SVO compound. Kittaka *et al.* studied the formation of SVO through the reaction of $V_2O_5 \cdot nH_2O$ and $AgNO_3$ solution in a wet system at room temperature and found that the reaction between $V_2O_5 \cdot nH_2O$ and $AgNO_3$ is so slow that several months for reaction are often required.[11] Sharma *et al.* reported the ion exchange synthesis of β-$AgVO_3$ by using organically intercalated vanadates as precursors.[12] Zhu *et al.* synthesized β-$AgVO_3$ nanowires using vanadium pentoxide powders and silver nitrate as reactants in the presence of 1,6-hexanediamine *via* a novel sonochemical route.[13] In addition, several kinds of β-$AgVO_3$ nanostructures have been synthesized through the hydrothermal process.[14−18]

However, to the best of our knowledge, it has not been reported hitherto that β-$AgVO_3$ nanoribbons can be yielded directly from reaction between V_2O_5 and $AgNO_3$ in aqueous solution. It is of great importance to develop simple, fast, and low-cost synthesis methods for control over the morphology of β-$AgVO_3$ from the viewpoint of its application.

Herein, we report a simple approach for high-yield synthesis of β-$AgVO_3$ nanoribbons by a hydrothermal reaction of bulky V_2O_5 and $AgVO_3$ powder in aqueous solution with the aid of pyridine. The direct transformation from the layered V_2O_5 to β-$AgVO_3$ nanoribbons can be achieved without undergoing valence change for V element. Controllable experiments have been carried out to investigate the growth mechanism of the β-$AgVO_3$ nanoribbons. The stability, electrical, and electrochemical performance of the β-$AgVO_3$ nanoribbons has been examined.

*Address correspondence to shyu@ustc.edu.cn.

Received for review November 30, 2008 and accepted February 15, 2009.

Published online February 20, 2009.
10.1021/nn800813s CCC: $40.75

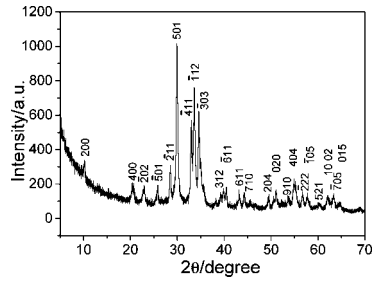

Figure 1. XRD pattern of the β-$AgVO_3$ nanoribbons prepared at 180 °C for 3 h.

RESULTS AND DISCUSSION

Morphology and Structure. The elegant β-$AgVO_3$ nanoribbons were synthesized through a hydrothermal route directly from a reaction of V_2O_5 and $AgNO_3$ in aqueous solution with the aid of the organic solvent pyridine at 180 °C for 3 h. Figure 1 shows the typical X-ray diffraction (XRD) pattern for the as-prepared β-$AgVO_3$ nanoribbons. All diffraction peaks can be indexed to the phase of β-$AgVO_3$ monoclinic structure [space group *I*2/*m* (No. 12)] (JCPDS card 29-1154). No peaks from other phases can be detected. In contrast, the (501) diffraction peak is the strongest one, while the strongest peak of β-$AgVO_3$ in the literature is the ($\bar{4}$11), indicating the possible preferential orientation of the β-$AgVO_3$ nanoribbons.

The low-magnification field emission scanning electron microscopy (FE-SEM) and transmission electron microscope (TEM) images in Figure 2a,b reveal that the as-prepared sample consists of highly flexible nanoribbons with lengths of at least several hundred micrometers. High-magnification FE-SEM images in Figure 2c,d show that the thickness and width of the appointed nanoribbons can be determined to be *ca.* 30 and 300 nm, respectively. In general, the nanoribbons have typical widths of 300−600 nm, thickness in the range of 30−60 nm, and lengths of 200−300 μm.

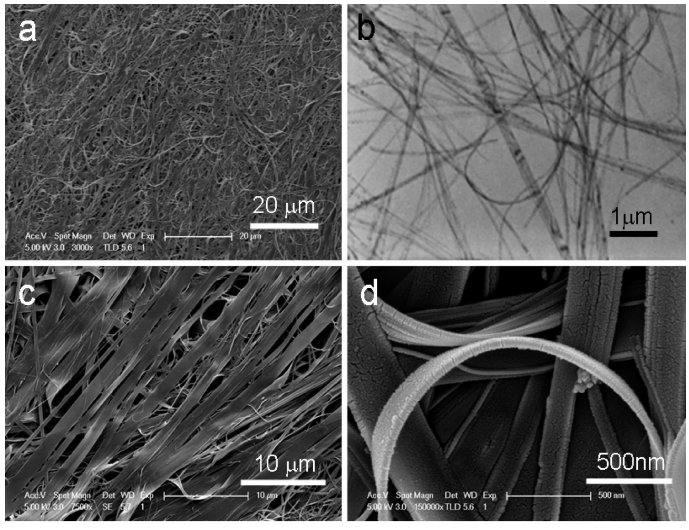

Figure 2. FESEM (a,c,d) and TEM (b) images of the β-$AgVO_3$ nanoribbons synthesized at 180 °C for 3 h. (a,b) Low-magnification SEM and TEM images; (c) high-magnification image; (d) typical image showing lateral surface of a single nanoribbon.

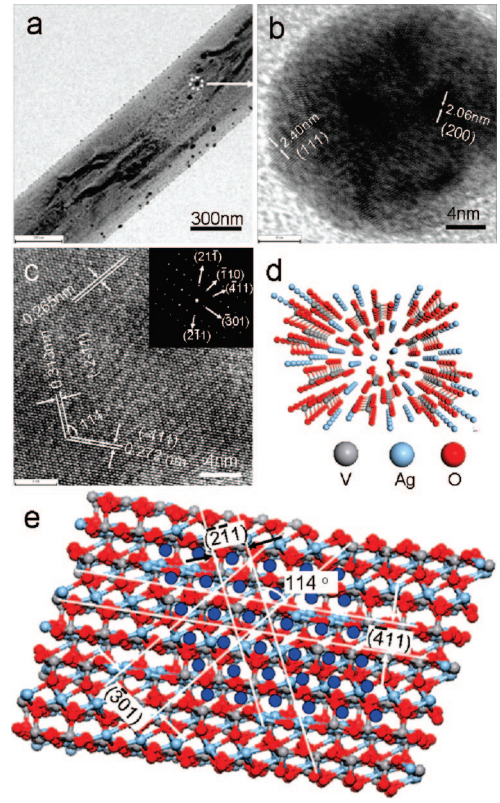

Figure 3. (a) TEM image of an individual β-$AgVO_3$ nanoribbon. (b,c) HRTEM images of different areas of the individual nanoribbon. Inset in c shows the corresponding SAED pattern taken along the [113] direction. (d) Schematic illustration of the β-$AgVO_3$ structure. Perspective view of $AgVO_3$ (1 × 5 × 3 cells): red balls, O; green balls, Ag; gray balls, V. (e) Schematic illustration of the surface structure of the as-synthesized β-$AgVO_3$ nanoribbons viewed from the [113] direction. The blue balls are dot matrix from (2̄1̄1) and (4̄11) planes in order to mark the (3̄01) plane.

The morphology and structure of the nanoribbons were further characterized by TEM, selected area electron diffraction (SAED) patterns, and high-resolution transmission electron microscope (HRTEM) analysis. There are some little particles with a diameter of *ca.* 20 nm on the surface of β-$AgVO_3$ nanoribbons (Figure 3a). The formation of these nanoparticles on the ribbons is due to the bombardment of high-energy electrons during the TEM observation. The number of the nanoparticles will rapidly increase with increasing exposure time of electron beam to the sample, which has been clearly observed as shown in Figure 4. Figure 3b displays the HRTEM image taken on a typical nanoparticle. The lattice spacings of 2.40 and 2.06 Å are in agreement with the values of the lattice spacings of the (111) and (200) planes of cubic Ag phase. Herein, *in situ* formation of Ag nanoparticles on the backbone of nanoribbons will provide an efficient route for the synthesis of composite catalysts directly without using a chemical reducing reaction between β-$AgVO_3$ and Cu coil.[16,19] The β-$AgVO_3$

nanoribbons with Ag nanoparticles reduced *in situ* have potential applications for Raman SERS detection and catalytic applications.[20]

HRTEM image in Figure 3c shows lattice spacings of *ca.* 2.72, 2.65, and 3.13 Å, corresponding to the lattice spacings of the $(\bar{4}11)$, $(\bar{3}01)$, and $(\bar{2}\bar{1}1)$ planes for monoclinic structure β-$AgVO_3$, respectively. The HRTEM pattern demonstrates that the ribbon structure of β-$AgVO_3$ is oriented along the $(\bar{3}01)$ plane. Meanwhile, the angle between the $(\bar{2}\bar{1}1)$ plane and $(\bar{4}11)$ plane is 114°, which is consistent with that calculated result according to its crystal structure. The corresponding SAED pattern taken along the [113] direction on the nanoribbon indicated the nanoribbon is single crystalline (inset in Figure 3c). The structure information of β-$AgVO_3$ nanoribbons from the HRTEM and SAED patterns can be well described *via* the schematic illustration of the surface structure viewed from the [113] direction (Figure 3e). Figure 3d illustrates the schematic structure of β-$AgVO_3$, in which Ag^+ cations are located between the vanadate layers in different types and directly influence the bond lengths of V and O.[14] The surface atom arrangement of the (113) face (along thickness direction) and $(\bar{3}01)$ face (lateral surface) of the silver vanadate nanoribbons may explain why the two faces can exist after reaction. It is believed that the relative growth rate of different crystal facets and the difference in the growth rates of various crystal facets result in different outlook of the crystallites. According to the structural characteristics of β-$AgVO_3$, the views along the (113) and $(\bar{3}01)$ planes indicate that there are more Ag atoms appearing on the planes (see Supporting Information Figure S2). Thus, the pyridine molecules have more chances to interact with the Ag atoms on these planes and reduce the reactive activity of these planes.

Figure 5a shows the Raman spectrum of the as-prepared β-$AgVO_3$ nanoribbons. Crystalline bulk $AgVO_3$ consists of polymeric metavanadate, $(VO_3)_n^{n-}$, corresponding to single or double chains composed of polymeric VO_4 units.[21] The strong band at 887 cm^{-1} may originate from either bridging V−O−Ag or O−V−O vibrations. The band at 845 cm^{-1} can be associated with the stretching vibrations of VO_3 groups in the $(V_2O_7)^{4-}$ ion. The band at 808 cm^{-1} can be assigned to stretching vibrations of the Ag−O−Ag bridges.[22] The bridging V−O−V bond in the polymeric metavandate chains is reflected by the 732 and 517 cm^{-1} bands, corresponding to the asymmetric and symmetric stretches, respectively. These peaks along with those located at 390, 340, 249, and 172 cm^{-1} are the clear signature of the $AgVO_3$, which is similar to that of the channel-structured silver vanadate reported by Bao *et al.*[14]

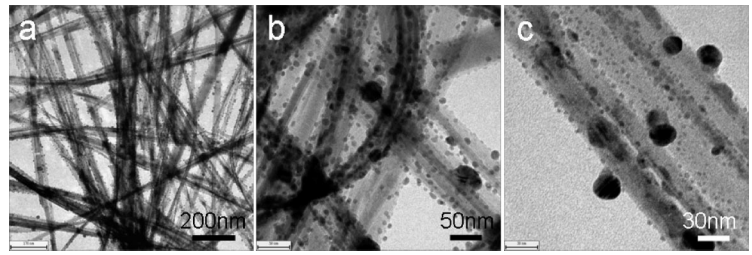

Figure 4. (a−c) TEM images of the as-prepared β-$AgVO_3$ nanoribbons under exposure to electron beam. Many tiny silver nanoparticles with a diameter less than 30 nm formed *in situ* on the surface of backbone of the nanoribbons after an exposure time of about 5 min.

The XPS analysis provided further information for the evaluation of the surface composition and purity of the product. The XPS survey spectrum in Figure 5b shows that the peak values at 284.5 eV can be readily assigned to the binding energies of C 1s. No peaks of other elements except C, O, Ag, and V were observed in the spectrum, indicating the high purity of this product. The two strong peaks at the Ag region of 367.5 and 373.5 eV are, respectively, assigned to Ag 3d(5/2) and Ag 3d(3/2), whereas the three peaks located at 516.6, 524.1, and 529.8 eV corresponded to V 2p(3/2), V 2p(1/2), and O 1s, respectively (Figure 5c,d). The atomic ratio of the Ag/V/O in $AgVO_3$ calculated from the peak area

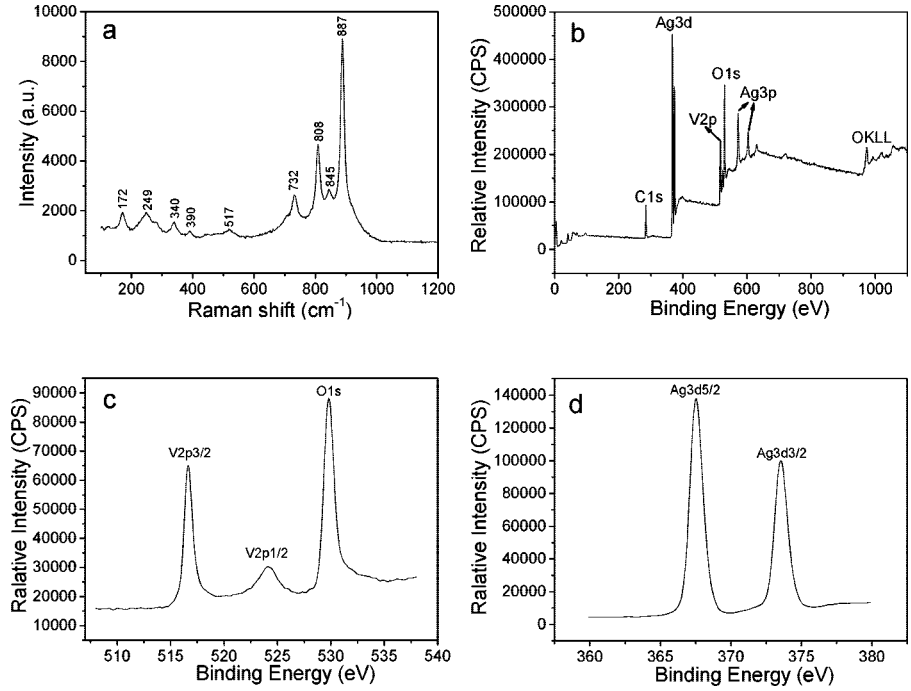

Figure 5. Raman scattering spectrum and XPS spectra of the β-$AgVO_3$ nanoribbons obtained at 180 °C for 3 h; (a) Raman spectrum; (b) XPS survey spectrum of the sample; (c) XPS spectra of the O 1s and V 2p regions; (d) XPS spectrum of the Ag 3d region.

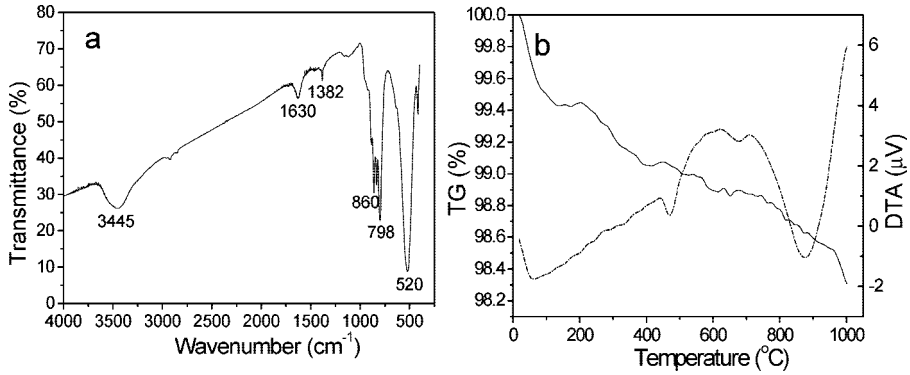

Figure 6. (a) FT-IR spectrum of the as-synthesized β-$AgVO_3$ nanoribbons by reaction of V_2O_5 with $AgVO_3$ in the presence of a small amount pyridine at 180 °C for 3 h; (b) TG and DTA analyses of the as-prepared nanoribbons.

is approximately 1:1:3, which is consistent with the given formula for $AgVO_3$ within the experimental errors.

Fourier transform infrared (FT-IR) spectrum in Figure 6a shows that there are characteristic absorption peaks at 798 and 520 cm^{-1} in the samples, which can be assigned as the symmetric and asymmetric stretching vibration peaks of the V−O band in the silver vanadate structure, respectively. The absorption bands at 860 cm^{-1} are assigned as V═O stretching mode. The band at 1382 cm^{-1} might be due to nitrate radical residue from the reactant. The bands at 3445 and 1630 cm^{-1} are the stretching of O−H and flexural vibrations of the O−H in free water, respectively.

Thermogravimetric (TG) analysis indicates that the as-prepared nanoribbons have very little weight loss from room temperature to 1000 °C in flowing nitrogen (below 1.5 wt %) in Figure 6b. The result is quite different from that reported by Mao *et al.*,[13] in which there is 27 wt % weight loss of β-$AgVO_3$ nanowires in the temperature range from 37 to 700 °C in flowing N_2 atmosphere. The TG curve of β-$AgVO_3$ nanoribbons reveals weight loss distributing in three sectors due to removal of physisorbed and chemisorbed water. The low-temperature sector (<120 °C) weight loss may be attributed to the loss of free water. The second weight loss, in the temperature range of 200 and 380 °C, is due to the loss of physically adsorbed water and coordinated water.[23] For the two low-temperature peaks, the weight losses were 0.55 and 0.37 wt %, respectively, as shown by the black curve in Figure 6b. Differential thermal analysis (DTA) in the dash-dot curve shown in Figure 6b shows that there are other main peaks: one endothermic peak centered at 470 °C, the other exothermic peak at 877 °C with no associated obvious weight loss; these may correspond to the phase transformation of silver vanadium oxide.[23] The TG-DTA analysis shows that the as-synthesized β-$AgVO_3$ nanoribbons have good thermal stability in nitrogen atmosphere.

Formation Mechanism of β-$AgVO_3$ Nanoribbons. The formation mechanism of the elegant β-$AgVO_3$ ribbon-like nanostructures has been investigated. In the present synthesis, neither templates nor surfactants are used in the reaction system. Figure 7 shows the schematic diagram of synthetic procedures. Procedure b is a typical synthesis process in which two reactants, $AgNO_3$ and V_2O_5, are directly added at one time into the autoclave. As a contrast experiment, the two reactants are also added in turn in the procedure a. As shown in the schematic diagram, the product is entirely the same from the two procedures, though the synthesis steps have some differences.

V_2O_5, an amphoteric oxide, is the most important compound of vanadium in the manufacture of sulfuric acid, and it can slightly dissolve in water due to hydrolysis. The orthorhombic crystal structure of V_2O_5 can be described as layers of VO_5 square pyramids that share edges and corners.[24] The sixth V−O bond in the *c*-direction consists of weak electrostatic interactions, which facilitate the insertion of various ions and molecules between the layers[25,26] (see Supporting Information Figure S1). From Figure 7, we can see that the V_2O_5 powder (0.45 mmol) can partly dissolve in 40 mL of distilled water and form aurantium suspended solution with pH 2.83. The pH value quickly reaches 6.71, and the mixture solution will be more transparent and becomes a colloid solution when 2 mL of pyridine (Py) is added into the suspension. This colloid solution is entirely transparent and will form a clear solution when it undergoes a hydrothermal treatment at 160 °C for 3 h. The pH value of the mixture solution is stabilized at 6.5−7.0 during the reaction process af-

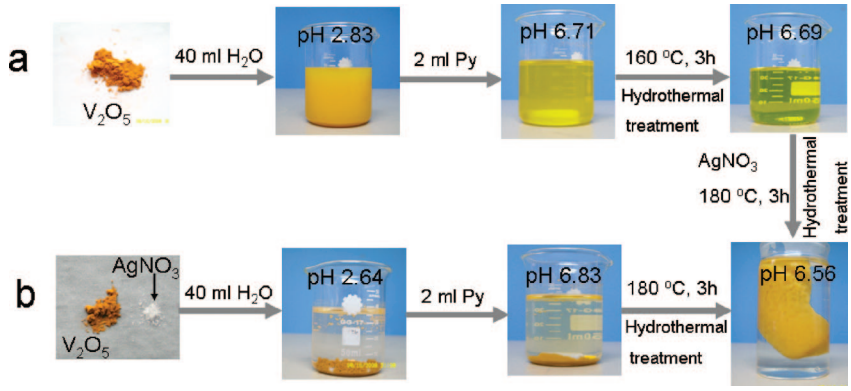

Figure 7. Schematic illustration of the synthesis procedure, including the photos and pH values at every stage. (a) Two kinds of reactants are added in turn. (b) Two kinds of reactants are added at one time.

ter pyridine is added. Thus, the overall chemical reaction involved in the hydrothermal synthesis can be briefly described by eqs 1−3.

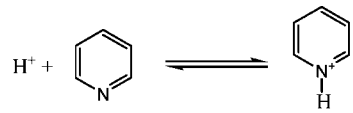

(1)

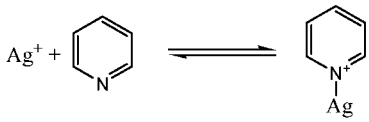

(2)

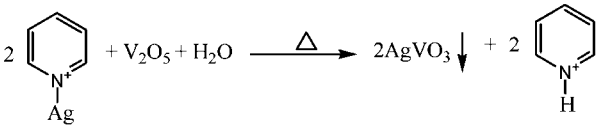

(3)

Pyridine is a simple and fundamentally important heterocyclic aromatic organic compound. It is structurally related to benzene, wherein one CH group in the six-membered ring is replaced by a nitrogen atom. The nitrogen atom on pyridine features a basic lone pair of electrons. Because this lone pair is not delocalized into the aromatic π-system, pyridine is basic with chemical properties similar to tertiary amines. Pyridine is protonated by reaction with acids from the reaction of eq 1 and forms a positively charged aromatic polyatomic ion called pyridinium cation, which is isoelectronic with benzene. The reaction as described eq 1 is similar to an acid−base buffer pair, so the pH value of the mixture solution can be stabilized in a small range. In reaction eq 2, the pyridinium cation of coordination between Ag^+ and Py can slow the reaction activity of silver ions. V_2O_5 powder will totally dissolve in solution with increasing temperature, and then good contact between silver ions in the pyridinium complex and VO_3^- can be gradually achieved. There is a competition between the Py and VO_3 group for the silver ion, and silver vanadate can be formed if the combining force of silver ion with VO_3^- is greater than that of silver ion and pyridine. As illustrated in eq 3, the pH value does not change largely, although new H^+ ions have been generated in the reaction process because the pyridinium cations have been produced immediately between the H^+ ions freshly formed and pyridine to stabilize the pH. This presumption has been validated by the experiment, similar to the procedure b, in which pH has been adjusted to 6.83 with 0.1 M NaOH aqueous solution before heating the autoclave, but without using pyridine. After the reaction, the pH value of the solution decreased to 5.80. At last, jelly-like product formed will fill up the whole inner Teflon liner of the autoclave (see the right lower picture in Figure 7).

The β-$AgVO_3$ nanoribbons prepared *via* the above procedure are flexible and can be easily curled at elevating temperature. Figure 8 shows FESEM images of silver vanadate loops formed after calcination of the β-$AgVO_3$ nanoribbons at 350 °C for 12 h in air. The long nanoribbons have mainly broken into many short slices, and a few nanoribbons curled into loops (Figure 8a). The typical curling loops can be clearly seen in magnified SEM images shown in Figure 8b−d. These microloops are very similar to self-coiling of $Ag_2V_4O_{11}$ nanobelts reported previously.[27]

The presence of pyridine is essential for the formation of β-$AgVO_3$ nanoribbons in present reaction system. We propose that pyridine plays an important role not only in stabilizing pH value but also in slowing the reaction because pyridine molecules can easily coordinate with silver ions to form pyridine salt. No nanoribbons can be obtained, and instead aggregated particles are obtained in the absence of pyridine, which could be due to a too fast reaction speed. The amount of pyridine has been varied from 1 to 20 mL. It has been found that the appropriate dosage of pyridine is *ca.* 2 mL in the present synthesis. FESEM images of as-synthesized silver vanadate in the presence of different dosage pyridine under other identical experimental conditions show that the ribbons and agglomerated particles were obtained when the amount of pyridine was 0.5 mL (see Supporting Information Figure S5a,b). While the amounts of pyridine added are 1 and 3 mL, respectively, long and short nanoribbons with inhomogeneity are synthesized (see Supporting Information Figure S5c−f). When 4 mL of pyridine is added, the yield of product is very low and a large amount of particles and a small amount of ribbons with a light gray color are obtained (see Supporting Information Figure S5g,h).

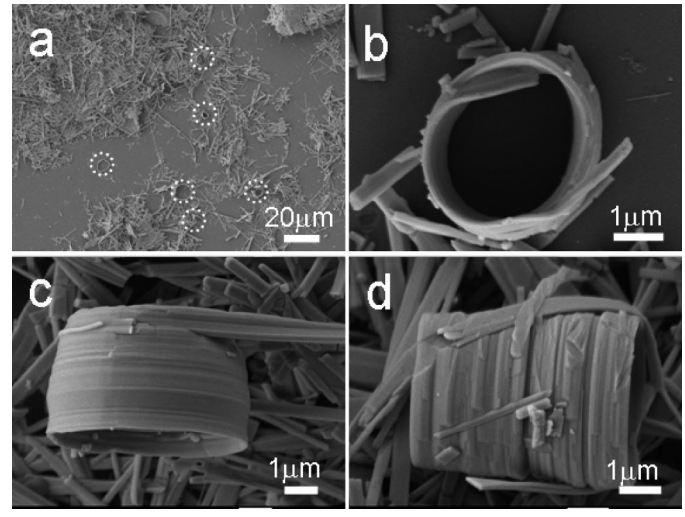

Figure 8. FESEM images of silver vanadate loops after annealing the sample at 350 °C for 12 h, which was prepared after hydrothermal treatment at 180 °C for 3 h. (a) General view at a low magnification; (b−d) typical highly curled loops found in the sample.

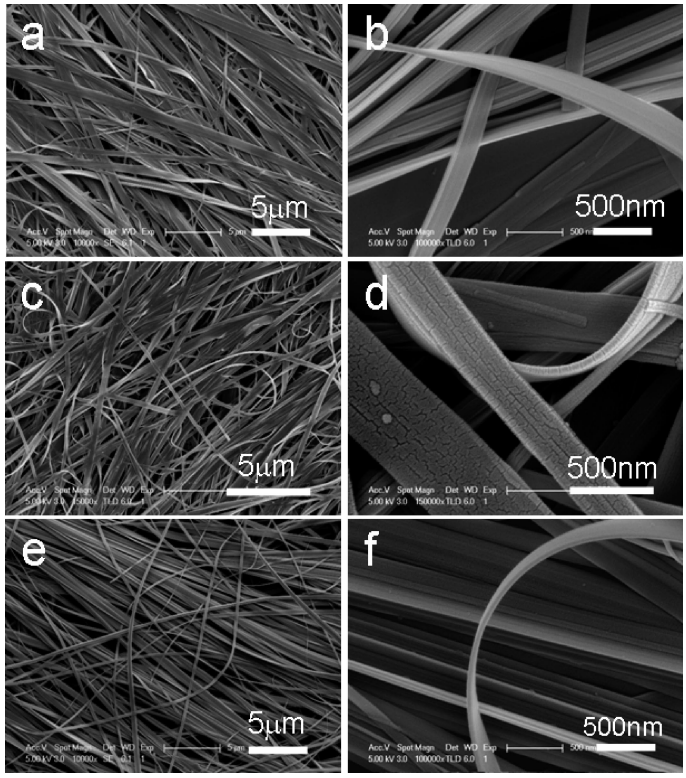

Figure 9. FESEM images of silver vanadate nanoribbons prepared at different temperature for 12 h: (a,b) 160 °C; (c,d) 180 °C; (e,f) 200 °C.

The monoclinic β-$AgVO_3$ phase is obtained when the amount of pyridine is 0.5 and 1 mL. While the amounts of pyridine added are 3 and 4 mL, the crystalline phase of the product is quite different from monoclinic β-$AgVO_3$. Thus, the dosage of pyridine used in the present reaction system plays an important role in controlling both the shape and phase formation (see Supporting Information Figure S6).

In addition, the formation of β-$AgVO_3$ nanoribbons is also dependent on reaction temperature and time. The reaction cannot take place when the temperature is below 140 °C. The products obtained at different temperature from 160 to 220 °C are all one-dimensional ribbon-like nanostructures (Figure 9). The products prepared at 180 and 200 °C can be indexed to pure monoclinic β-$AgVO_3$ phase, while the mixture phases of α-$AgVO_3$ and β-$AgVO_3$ are obtained at 160 °C (see Supporting Information Figure S3), which are agreement with the results reported in the literature.[28] In a typical synthesis procedure (temperature is kept at 180 °C), when the reaction time is more than 2 h, elegant nanoribbons can be obtained; while reaction time is as short as 1 h, long nanowires are produced (see Supporting Information Figure S4).

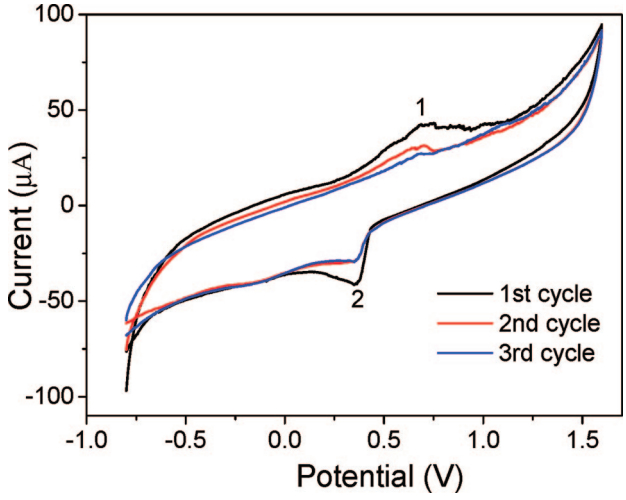

Figure 10. Three successive cyclic voltammograms of the β-$AgVO_3$ nanoribbons in 0.10 mol · L^{-1} KNO_3, which were prepared at 180 °C for 3 h. The scan rate is 20 mV/s.

Electrochemical and Electrical Properties of β-$AgVO_3$ Nanoribbons. Electrochemical and electrical properties of β-$AgVO_3$ nanoribbons have been investigated. Figure 10a shows the three successive cyclic voltammograms of β-$AgVO_3$ nanoribbons in 0.10 mol · L^{-1} KNO_3 aqueous solution by linear scan voltammetry. From the patterns, it can be seen that the peaks of the three cycles are all similar. Noticeably, peaks 1 and 2 in the first cyclic voltammogram are stronger and then fall off in the second and third cyclic voltammograms, but the positions do not change. This phenomenon can be explained by the fact that the sample adsorbed in the electrode surface reduces with an increasing number of the cycle. The anode peak (at 0.71 V) and the cathodic peak (at 0.36 V) on the curve can be designated to two reversible redox couples: Ag^+/Ag^0 and VO_2^+/V^{2+}.

The electrical conductivity property has seldom been reported for an individual single-crystal β-$AgVO_3$ nanoribbon. Recently, Li *et al.* have reported the electrical conductivity of the sub-micrometer-sized β-$AgVO_3$ ribbons with channel structure.[14] Here, we preliminarily discussed the electrical conductivity property of an individual single-crystal β-$AgVO_3$ nanoribbon by scanning the bias voltage at room temperature and ambient air condition. Owing to the existence of Ag^+ cations between the vanadate layers in the β-$AgVO_3$ structure, the prepared β-$AgVO_3$ nanoribbons are expected to have a good electrical conductivity for potential applications in microelectrodes or nanodevices. The current−voltage ($I-V$) curve of a single β-$AgVO_3$ nanoribbon at room temperature is shown in Figure 11a. A schematic view and the SEM image of an individual β-$AgVO_3$ nanoribbon electrode are shown in the insets of Figure 11a. From Figure 11a, it is clear that the bottom-contacted device exhibits nonlinear and symmetric current/voltage ($I-V$) characteristics for bias voltages in the range of −6 to 6 V. The curve is reproducible, and no large fluctuations are observed even in the high bias region, indicating that the device is stable.

Figure 11b displays the $I-V$ plot of the bulk β-$AgVO_3$ pellet (made *via* a pressed disk method; *i.e.*, the powder of β-$AgVO_3$ nanoribbons was pressed under a pressure of 15 atm · cm^{-2}). It mainly shows ohmic electrical

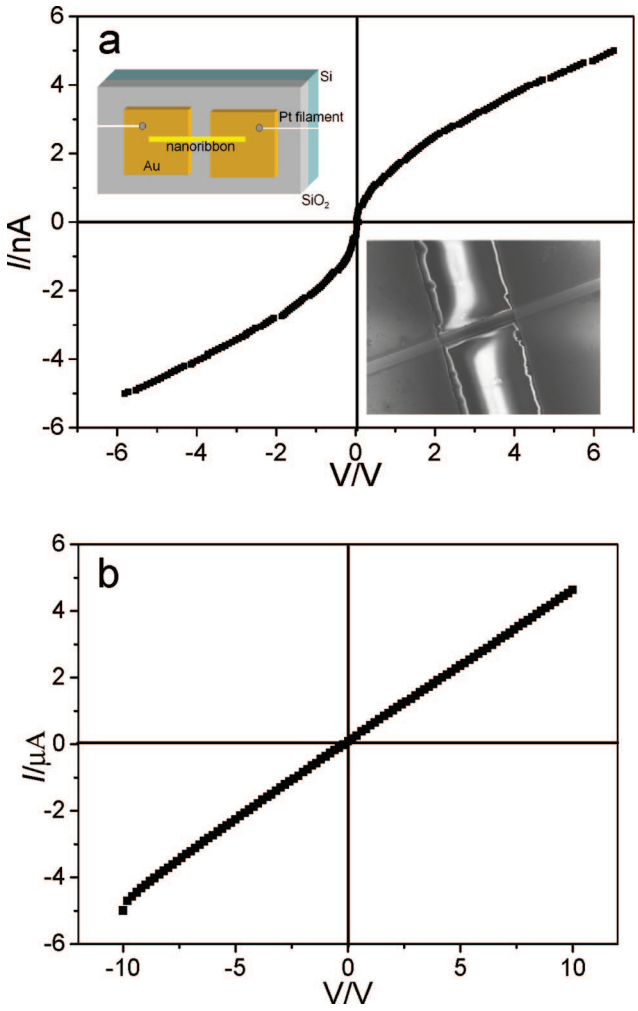

Figure 11. (a) *I*−*V* curve of the gold electrode with an individual β-$AgVO_3$ nanoribbon. Insets: schematic view (top left) and the SEM image of the individual nanoribbon electrode (bottom right). (b) *I*−*V* plot of bulk β-$AgVO_3$ pellet (made *via* a pressed disk method; *i.e.*, the powder of β-$AgVO_3$ nanoribbons was pressed under a pressure of 15 atm · cm^{-2}).

transport. The bulk electrical behavior is different from the individual β-$AgVO_3$ nanoribbon, which may be explained by the poor orientation of individual β-$AgVO_3$ nanoribbons in the bulk state.

CONCLUSION

In conclusion, we have developed a facile route for the synthesis of elegant and superlong β-$AgVO_3$ nanoribbons with widths of 300−600 nm, thicknesses of *ca.* 40 nm, and lengths of 200−300 μm *via* mild hydrothermal reaction without using any surfactant in a pyridine-mediated solution. Pyridine not only plays a coordination agent role for Ag^+ and H^+ at initial reaction stage but also provides a stable pH value in subsequent reaction because of the formation of the pyridinium cation. The β-$AgVO_3$ nanoribbons prepared *via* the above procedure are flexible and can be curled at elevated temperature. The TG and DTA analysis shows that the β-$AgVO_3$ nanoribbons as-synthesized have good thermal stability. The electrical conductivity property of an individual single-crystal β-$AgVO_3$ nanoribbon exhibits nonlinear and symmetric current/voltage (*I*−*V*) characteristics for bias voltages in the range of −6 to 6 V for the bottom-contacted device. In addition, exposure of the nanoribbons to electron beam will easily result in the formation of Ag nanoparticles embedded *in situ* on the backbone of the nanoribbons, making the nanoribbons act as efficient catalyst support, which will find applications either in SERS detections of organic molecules or as catalysts.

METHODS

Materials. All chemicals are analytical grade. Vanadium pentaoxide (V_2O_5) and silver nitrate ($AgNO_3$) were purchased from Shan Tou Xi Long Chemical Factory and Shanghai Chemical Reagent Co. Ltd., respectively. Pyridine and ethanol were purchased from Sinopharm Chemical Reagent Co., Ltd. All reagents were used as received, without further purification.

Synthesis of β-$AgVO_3$ Nanoribbons. The β-$AgVO_3$ nanoribbons were synthesized through a hydrothermal route by reaction of V_2O_5 with $AgNO_3$ in a Teflon-lined autoclave. In a typical procedure, 0.0765 g of $AgNO_3$, 0.0818 g of V_2O_5, and 40 mL of distilled were mixed together in a Teflon-lined stainless-steel autoclave with a volume capacity of 50 mL. Then 2 mL of pyridine was also dropwise added into the autoclave under vigorous stirring. The mixed solution displayed a color change from brick red to light yellow when pyridine is injected. After 30 min, the reaction mixture formed a homogeneous yellow suspension. The autoclave was sealed and maintained at 180 °C for 3 h, then cooled to room temperature naturally. The obtained gel state pale yellow solids, which overflowed the all inner lining, were collected by centrifuging the reaction mixture; the particles were then washed with distilled water and absolute ethanol several times each and dried in a vacuum at 60 °C for 6 h for further characterization.

Characterization. The phase purity of the as-prepared samples was examined by X-ray diffraction (XRD) using a Philips X'Pert PRO SUPER X-ray diffractometer equipped with graphite monochromatized Cu Kα radiation (λ = 1.54178 Å). To obtain further evidence for the purities and compositions of the as-prepared products, the X-ray photoelectron spectra (XPS) were applied, which were recorded on an ESCALab MKII X-ray photoelectron spectrometer, using Al Ka radiation as the exciting source. Raman spectra were performed with 488 nm laser excitation with a micro-Raman system, which was modified by coupling an Olympus microscope to a Spex 1740 spectrometer with a CCD detector. Scanning electron microscopy (SEM) and field emission scanning electron microscopy (FE-SEM) were applied to investigate the size and morphology and were carried out with a Hitachi X-650 scanning electron microanalyzer and a field emission scanning electron microanalyzer (JEOL-6700F), respectively. Transmission electron microscope (TEM) images were taken with a Hitachi H-800 transmission electron microscope at an acceleration voltage of 200 kV. High-resolution transmission electron microscope (HRTEM) analysis and selected area electron diffraction (SAED) patterns were performed on a JEOL-2010 transmission electron microscope. Thermogravimetric analysis (TGA) and differential thermal analysis (DTA) were carried out on

a TGA-60 thermal analyzer (Shimadzu Corporation) with a heating rate of 10 °C/min in flowing nitrogen. FT-IR (MAGNA-IR 750, Nicolet Instrument Co. USA) was dealt with dried powder. Electrochemical experiments were performed on an EG&G PAR Model 283 potentiostat/galvanostat.

Electrical conductivity of an individual nanoribbon was carried out on the Agilent E5270 I-V parametric measurement system. To make electrical contact with a single β-$AgVO_3$ nanoribbon, a diluted aqueous suspension of nanoribbons was stochastically dropped and dried on an oxidized silicon substrate, on which contacts of gold had been evaporated through a shadow mask in an early operation (photoetching method). The spacing intervals among gold contacts are 10 μm (see inset in Figure 11a). Two platinum wire electrodes were derived from the two gold contact dots with silver paste.

Acknowledgment. This work is supported by the National Science Foundation of China (NSFC) (Grants 50732006, 20621061, and 20671085), 2005CB623601, the Chinese Postdoctoral Science Foundation (20080430775), and the Partner-Group of the Chinese Academy of Sciences-Max Planck Society. We thank Prof. Kai-Bin Tang for his helpful discussion on the structural analysis.

Supporting Information Available: Figures S1−S6. This material is available free of charge *via* the Internet at http://pubs.acs.org.

REFERENCES AND NOTES

1. Pan, Z. W.; Dai, Z. R.; Wang, Z. L. Nanobelts of Semiconducting Oxides. *Science* **2001**, *291*, 1947–1949.
2. Maiti, A.; Rodriguez, J. A.; Law, M.; Kung, P.; McKinney, J. R.; Yang, P. D. SnO_2 Nanoribbons as NO_2 Sensors: Insights from First Principles Calculations. *Nano Lett.* **2003**, *3*, 1025–1028.
3. Law, M.; Sirbuly, D. J.; Johnson, J. C.; Goldberger, J.; Saykally, R. J.; Yang, P. D. Nanoribbon Waveguides for Subwavelength Photonics Integration. *Science* **2004**, *305*, 1269–1273.
4. Wang, Z. L. The New Field of Nanopiezotronics. *Mater. Today* **2007**, *10*, 20–28.
5. Chen, J. Y.; Wiley, B. J.; Xia, Y. N. One-Dimensional Nanostructures of Metals: Large-Scale Synthesis and Some Potential Applications. *Langmuir* **2007**, *23*, 4120–4129.
6. Shi, S. F.; Cao, M. H.; He, X. Y.; Xie, H. M. Surfactant-Assisted Hydrothermal Growth of Single-Crystalline Ultrahigh-Aspect-Ratio Vanadium Oxide Nanobelts. *Cryst. Growth Des.* **2007**, *7*, 1893–1897.
7. Cao, A. M.; Hu, J. S.; Liang, H. P.; Wan, L. J. Self-Assembled Vanadium Pentoxide (V_2O_5) Hollow Microspheres from Nanorods and Their Application in Lithium-Ion Batteries. *Angew. Chem., Int. Ed.* **2005**, *44*, 4391–4395.
8. Whittingham, M. S. Lithium Batteries and Cathode Materials. *Chem. Rev.* **2004**, *104*, 4271–4301.
9. Liu, J.; Wang, Y.; Peng, Q.; Li, Y. Vanadium Pentoxide Nanobelts: Highly Selective and Stable Ethanol Sensor Materials. *Adv. Mater.* **2005**, *17*, 764–767.
10. Takeuchi, K. J.; Marschilok, A. C.; Davis, S. M.; Leising, R. A.; Takeuchi, E. S. Silver Vanadium Oxides and Related Battery Applications. *Coord. Chem. Rev.* **2001**, *283*, 219–221.
11. Kittaka, S.; Yata, Y.; Matsuno, K.; Nishido, H. Interaction of Ag Ions with a Vanadium Pentoxide Hydrate—Formation of Silver Vanadate at Low Temperature. *J. Mater. Sci.* **2000**, *35*, 2185–2192.
12. Sharma, S.; PanthÖfer, M.; Jansen, M.; Ramanan, A. Ion Exchange Synthesis of Silver Vanadates from Organically Templated Layered Vanadates. *Mater. Chem. Phys.* **2005**, *91*, 257–260.
13. Mao, C. J.; Wu, X. C.; Zhu, J. J. Large Scale Preparation of β-$AgVO_3$ Nanowires Using a Novel Sonochemical Route. *J. Nanosci. Nanotechnol.* **2008**, *8*, 3203–3207.
14. Bao, S. J.; Bao, Q. L.; Li, C. M.; Chen, T. P.; Sun, C. Q.; Dong, Z. L.; Gan, Y.; Zhang, J. Synthesis and Electrical Transport of Novel Channel-Structured β-$AgVO_3$. *Small* **2007**, *3*, 1174–1177.
15. Liu, Y.; Zhang, Y. G.; Hu, Y. H.; Qian, Y. T. Hydrothermal Synthesis of Single-Crystal β-$AgVO_3$ Nanowires and Ribbon-like Nanowires. *Chem. Lett.* **2005**, *34*, 146–147.
16. Shao, M-W.; Lu, L.; Wang, H.; Wang, S.; Zhang, M. L.; Ma, D. D. D.; Lee, S. T. An Ultrasensitive Method: Surface-Enhanced Raman Scattering of Ag Nanoparticles from β-Silver Vanadate and Copper. *Chem. Commun.* **2008**, 2310–2312.
17. Li, M.; Shao, M. W; Ban, H. Z.; Wang, H.; Gao, H. Z. Synthesis of Ultra-long β-$AgVO_3$ Nanoribbon Bundles and Measurement of Their Conductivity. *Solid State Ionics* **2007**, *178*, 775–777.
18. Zhang, S. Y.; Li, W. Y.; Li, C. S.; Chen, J. Synthesis, Characterization, and Electrochemical Properties of $Ag_2V_4O_{11}$ and $AgVO_3$ 1-D Nano/Microstructures. *J. Phys. Chem. B* **2006**, *110*, 24855–24863.
19. Liu, S. W.; Wang, W. Z.; Zhou, L.; Zhang, L. S. Silver Vanadium Oxides Nanobelts and Their Chemical Reduction to Silver Nanobelts. *J. Cryst. Growth* **2006**, *293*, 404–408.
20. Li, G. C.; Chao, K.; Ye, C. S.; Peng, H. R. One-Step Synthesis of Ag Nanoparticles Supported on $AgVO_3$ Nanobelts. *Mater. Lett.* **2008**, *62*, 735–738.
21. Tian, H. J.; Wachs, I. E.; Briand, L. E. Comparison of UV and Visible Raman Spectroscopy of Bulk Metal Molybdate and Metal Vanadate Catalysts. *J. Phys. Chem. B* **2005**, *109*, 23491–23499.
22. Lewandowska, R.; Krasowski, K.; Bacewicz, R.; Garbarczyk, J. E. Studies of Silver-Vanadate Superionic Glasses Using Raman Spectroscopy. *Solid State Ionics* **1999**, *119*, 229–234.
23. Xiong, C. R.; Aliev, A. E.; Gnade, B.; Balkus, K. J. Fabrication of Silver Vanadium Oxide and V_2O_5 Nanowires for Electrochromics. *ACS Nano* **2008**, *2*, 293–301.
24. Murphy, D. W.; Christian, P. A.; DiSalvo, F. J.; Waszczak, J. V. Lithium Incorporation by Vanadium Pentoxide. *Inorg. Chem.* **1979**, *18*, 2800.
25. Whittingham, M. S. Role of Ternary Phases in Cathode Reactions. *J. Electrochem. Soc.* **1976**, *123*, 315–320.
26. Chan, C. K.; Peng, H. L.; Twesten, R. D.; Jarausch, K.; Zhang, X. F.; Cui, Y. Fast, Completely Reversible Li Insertion in Vanadium Pentoxide Nanoribbons. *Nano. Lett.* **2007**, *7*, 490–495.
27. Shen, G. Z.; Chen, D. Self-Coiling of $Ag_2V_4O_{11}$ Nanobelts into Perfect Nanorings and Microloops. *J. Am. Chem. Soc.* **2006**, *128*, 11762–11763.
28. Kittaka, S.; Matsuno, K.; Akashi, H. Crystal Structure of α-$AgVO_3$ and Phase Relation of $AgVO_3$. *J. Solid State Chem.* **1999**, *142*, 360–367.